Soft Matter

View Online
Dynamic Article Links

Cite this: *Soft Matter*, 2011, **7**, 9140

www.rsc.org/softmatter

PAPER

Kinetically controlled self-assembly of monolayered micelle films of P(S-*b*-4VP) on bare and PS-grafted substrates†

Chih-Yao Chang,[a] Pin-Jiun Wu[b] and Ya-Sen Sun*[a]

Received 9th June 2011, Accepted 18th July 2011
DOI: 10.1039/c1sm06082a

Published on 15 August 2011 on http://pubs.rsc.org | doi:10.1039/C1SM06082A
Downloaded by Synchrotron Radiation Library on 23 September 2011

We investigated the temporal evolution of micellar nanostructures in solvent-annealed poly(styrene-*block*-4-vinylpyridine) P(S-*b*-4VP) monolayer films on bare and PS-grafted substrates under tetrahydrofuran (THF) vapor. The size of end-grafted PS homopolymers on Si substrates has a large effect on the kinetics of transitions between spherical and cylindrical micelles at the early and intermediate stages of solvent annealing. At these stages, cylindrical micelles developing *via* micellar merger were dominant over spherical micelles growing *via* micellar splitting on substrates grafted with a layer of short PS brushes (PS_{4k}–SiO_x/Si). On substrates having an attractive surface (SiO_x/Si) or a grafted layer of long PS chains (PS_{19k}–SiO_x/Si), the dominant surface morphology was inverted through the dominance of micellar splitting. Upon solvent annealing for a given interval in THF, micellar structures existed as a single morphology of cylindrical micelles on PS_{4k}–SiO_x/Si, but appeared as spherical micelles on SiO_x/Si and PS_{19k}–SiO_x/Si. On immersion of these micelles in ethanol to give rise to opening of the micelles, dimple-like nanopores in hexagonal arrays were induced on SiO_x/Si but stripe-like nanogrooves were induced on PS_{4k}–SiO_x/Si. We demonstrate a novel method of kinetically controlled hierarchical self-assembly of P(S-*b*-4VP) micellar species. On combining the chemical micropatterning of the grafted layer of PS brushes with UV/ozone etching, we prepared P(S-*b*-4VP) films that have dimple-like nanopores and stripe-like nanogrooves coexisting with a micro-scale order within the same monolayer.

Introduction

Amphiphilic block copolymer (a-BCP) micelles used as nanostructured materials continue to be the focus of intense research because they offer diverse and versatile benefits for applications such as templates to guide silicon-surface chemistry[1] and for the fabrication of nanometre-sized functional materials,[2–13] and nanoporous membranes for separation and filtration.[14,15] A key requirement to implement these applications is the ability to control the spatial orientation, ordering and morphological diversity of a-BCP micelles.

Much effort has been devoted to achieve long-range order of spherical micelles or vertically oriented cylinders in hexagonal arrays upon self-assembly by annealing thin films in the vapor of a selective solvent[16–18] or directed assembly within a topographic pattern,[19] but little attention has been paid to the morphological diversity of micelles or the hierarchical self-assembly of various micelles in thin films. Experiments have shown that a-BCP in a selective solvent form spherical micelles, depending on the nature of interactions between an a-BCP and a solvent.[20] The spherical micelle generally consists of a central core with one compact block and an outer corona with an extended, swollen block. On spin-coating a solution of spherical micelles on solid substrates, the rapid evaporation of a solvent during spin-coating inevitably produces frozen morphologies of a-BCP. A single morphology of spherical micelles thus exists on substrates despite the volume fraction of the constituted block being symmetric or slightly asymmetric in the bulk state of the melt. Unless there is exposure to the vapor of a neutral solvent[3,21,22] or thermal annealing at a high temperature[12] is imposed on the spherical micelles so as to grow parallel-oriented cylinders, the spheres develop steadily in most cases. Even though implementing further a solvent treatment or thermal annealing to grow parallel cylindrical micelles, a single morphology persists in the plane of the substrates.

Kim *et al.* found a surface-morphological evolution of poly (styrene-*block*-4-vinylpyridine) P(S-*b*-4VP) thin films of monolayer thickness as a function of annealing duration in THF.[23] They identified two mechanisms of micellar growing—merging of spherical micelles to form cylindrical micelles *via* fusion at early stages of solvent annealing, and splitting of cylindrical micelles to grow spherical micelles *via* fission at the later stage;

[a]*Department of Chemical and Materials Engineering, National Central University, Taoyuan, 32001, Taiwan. E-mail: yssun@cc.ncu.edu.tw*
[b]*National Synchrotron Radiation Research Center, Hsinchu, 30077, Taiwan*

† Electronic supplementary information (ESI) available: Reflection optical micrographs and AFM topographic images of as-spun films from a solution (0.1 mass%) (Fig. S1). Cross-sectional profiles of the AFM topographies (Fig. S2). AFM topographic images of as-spun and solvent-annealed micelles with a small surface coverage on PS_{4k}–SiO_x/Si and PS_{19k}–SiO_x/Si (Fig. S3). See DOI: 10.1039/c1sm06082a

This journal is © The Royal Society of Chemistry 2011

View Online

Published on 15 August 2011 on http://pubs.rsc.org | doi:10.1039/C1SM06082A
Downloaded by Synchrotron Radiation Library on 23 September 2011

cylindrical micelles or spherical ones were thus obtained separately, depending on the time scale of exposure of thin films to solvent vapor. They found also that the rate of micelle–micelle fusion depended on the length of PS corona chains and on the mobility of P4VP core chains; they demonstrated a strategy to achieve ordered arrays of micelles within a topographic pattern by solvent annealing for various intervals, but only a single morphology of micelles (either cylinders or spheres) existed within the monolayer.

We have investigated the temporal evolution of micellar nanostructures in solvent-annealed P(S-*b*-4VP) monolayered films on bare silicon substrates and PS-grafted substrates under THF vapor. We found that the chain length of the PS layer with chain ends grafted onto a silicon substrate and interfacial interactions play important roles in controlling the rate of transitions between spherical and cylindrical micelles through fusion or fission. Here we first show the temporal evolution of surface morphologies of P(S-*b*-4VP) thin films of initially disordered spherical micelles that incompletely or completely cover bare Si substrates (SiO_x/Si). Next we show the temporal evolution of micellar nanostructures on substrates grafted with a layer of PS homopolymers. Surface-grafted substrates of two molar masses were used (denoted briefly as PS_{4k}–SiO_x/Si and PS_{19k}–SiO_x/Si) to assess the effect of the chain length of grafted PS. Achieving a concurrent presence of micelles of two kinds on the same layer registering with a macroscopic order on substrates has not yet been demonstrated. We demonstrate a novel method of kinetically controlled hierarchical self-assembly of P(S-*b*-4VP) monolayered films on a chemically micro-patterned substrate, which was fabricated through selective etching of the grafted layer of PS brushes with ultraviolet light and ozone.

Experimental

Materials

Hydroxyl-terminated polystyrenes of disparate molar mass were used for surface modification (PS_{4k}–OH: $M_n = 4$ kg mol^{-1}, index of polydispersity $I_p = 1.09$ (Polymer Source, Inc.), and PS_{19k}–OH: $M_n = 19$ kg mol^{-1}, $I_p = 1.19$). P(S-*b*-4VP) ($M_n = 44$ kg mol^{-1}, $f_{ps} = 50\%$ and $f_{P4VP} = 50\%$, $I_p = 1.09$) block copolymer was purchased (Polymer Source, Inc.) and used as received.

Surface modification of substrates with spin coating

Bare silicon wafers were cleaned in a piranha solution (3 : 7 v/v 30% H_2O_2 : H_2SO_4) for 40 min, rinsed with deionized water, and dried under flowing N_2. For substrates with surface modification grafted with PS brushes, PS–OH solutions (1 mass% in toluene) were spin-coated (1000 rpm, 1 min) on silicon wafers. The irreversibly grafted layers resulted from annealing (190 °C for 3 days) spin-coated films on hydroxylated silicon wafers under vacuum. Non-grafted materials were removed on sonication in toluene, followed by drying the substrates under flowing N_2.

Film preparation, annealing and chemical micropatterning with UV light and ozone

P(S-*b*-4VP) powders were dissolved in a mixture (70/30) of toluene and THF at 70 °C for 2 h to yield 0.1 and 0.5 mass% solutions. P(S-*b*-4VP) films were spread on substrates *via* spin coating (2000 rpm, 60 s) from mixed solvents of toluene/THF. The thin films were placed in a chamber of saturated THF vapor for varied periods (15–360 min) of solvent annealing, which was performed at a maintained temperature of 26 °C with a humidity less than 20%. Surface-reconstructed films were prepared on immersion of solvent-annealed films in ethanol for 20 min. Chemical micropatterning of PS brushes was performed *via* selective etching with ultraviolet light and ozone (10 min) with a Cu TEM grid shadow mask.

Characterization

To determine micellar nanostructures, we investigated the surface of the thin films with an atomic-force microscope (AFM, SPA400 Seiko) in the tapping mode and with a high-resolution field-emission scanning electron microscope (HR-FESEM, JEOL JSM-7600F) with a field emission source of energy 10 keV. AFM images were recorded with scan ranges between 1 μm × 1 μm and 2 μm × 2 μm. We used aluminium-coated silicon cantilevers (length 150 μm, width 26 μm, thickness 300 μm); the force coefficient was approximately 7.4 N m^{-1} and the resonant frequency was 160 kHz. The micropatterned morphology of P(S-*b*-4VP) thin films was observed with an optical microscope (OM, Olympus BX-BLA2) in the reflection mode. The thickness of films was measured through X-ray reflectivity (X-ray source $\lambda =$ 1.54 Å, XR, Bruker, D8 SSS) and a synchrotron source ($\lambda = 1.55$ Å, beamline 17B at National Synchrotron Radiation Research Center, NSRRC, Hsinchu). To probe the orientation and ordering of nanodomains, we performed GISAXS experiments at beamline BL23A of NSRRC. The configuration of the GISAXS at BL23A is described in detail elsewhere.[24]

Results and discussion

Effect of surface coverage on the temporal evolution of micelles of P(S-*b*-4VP) thin films on SiO_x/Si under solvent vapor

First we show the structural evolution of spherical micelles of P(S-*b*-4VP) on SiO_x/Si under solvent annealing in THF. THF is a slightly selective solvent: it is an effective solvent for the PS block, but a poor solvent for the P4VP block. Spin-coating from dilute solutions of 0.1 mass% led to an incomplete coverage of the surface of the substrate with disordered micelles. This incomplete surface coverage displays as various "dewetting" morphologies on a micro-scale shown in the optical micrographs (see Fig. S1 in the ESI†). During solvent annealing, the structural details particularly at the polymer–substrate interface are clearly visualized. As shown in Fig. 1a, before solvent annealing the as-spun film on SiO_x/Si reveals the morphology of spherical micelles, of dimension in the range 25–29 nm. As only one layer of spherical micelles was deposited on SiO_x/Si, the thickness of the layer depended on the dimension of spherical micelles (see Fig. S2 in the ESI†). As only a small amount of spherical micelles was deposited on SiO_x/Si from such a dilute solution of 0.1 mass %, upon exposure to THF vapors most micelles disintegrated to form a wetting monolayer, displaying as a featureless surface in the AFM phase images (see Fig. 1c–f). The height analysis of the AFM topographies demonstrates that the thickness of the wetting layer is approximately 3–4 nm (Fig. S2 in the ESI†). This

View Online

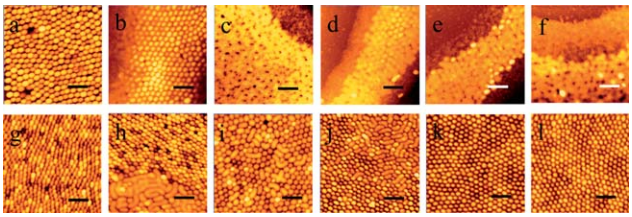

Fig. 1 AFM topographic images (1 μm × 1 μm) of P(S-*b*-4VP) thin films self-assembled on SiO_x/Si. Thin films were prepared on spin coating from 0.1 mass% (top row of images) and 0.5 mass% (bottom row of images) solutions in a toluene/THF solvent mixture. The topographic images were recorded (a and g) before and after P(S-*b*-4VP) films were subjected to solvent annealing for different periods: (b and h) 30, (c and i) 60, (d and j) 120, (e and k) 240, and (f and l) 300 min (scale bar: 200 nm).

Published on 15 August 2011 on http://pubs.rsc.org | doi:10.1039/C1SM06082A
Downloaded by Synchrotron Radiation Library on 23 September 2011

observation indicates that a strong affinity between the pyridine groups of P4VP chains and the hydroxyl surface of the bare silicon wafer results in the preferential formation of the wetting layer of P(S-*b*-4VP) chains with the P4VP blocks facing SiO_x/Si but the PS blocks facing outward to the air, in agreement with recent observations.[18]

In Fig. 1b, as the wetting monolayer develops, the diameter of micelles decreases. A scrutiny of the AFM images indicates an additional layer covering the wetting layer when micelles decrease in size until they completely disappear on solvent annealing for 60 min or longer (Fig. 1c–f). Gradual adsorption of P(S-*b*-4VP) chains by the attractive surface of SiO_x/Si to form the wetting layer from spherical micelles hence decreases the size of the micelles. As their size is less than the dimension required for forming a stable micelle, the immediate disintegration of all spherical micelles produces an additional layer of unimer chains. The time scale of such disintegration of micelles is sufficiently small that it is not achievable to assume the same conformation as those in the wetting layer through a substantial arrangement of unimer chains. The AFM images of P(S-*b*-4VP) films with protracted annealing in THF thus reveal a dual-layer morphology, of which the bottom layer displays a featureless surface and the top layer displays a patchy surface; the patchy layer has a thickness of approximately 5 nm (Fig. S2 in the ESI†). The overall thickness of the dual-layer structure is less than that for as-spun micelles. This result indicates that, in the presence of interfacial interactions of P4VP with SiO_x/Si, solvent annealing imposed on the spherical micelles that were spun from 0.1 mass% solutions onto SiO_x/Si results in not only a transition from spherical micelles to dual layers but also a variable thickness.

Thin films of P(S-*b*-4VP) with a complete surface coverage of spherical micelles were prepared on spin coating 0.5 mass% solutions in a toluene/THF solvent mixture onto SiO_x/Si substrates. The structural evolution between spherical and cylindrical micelles as a function of time is shown in Fig. 1g–l. For a complete coverage of SiO_x/Si with disordered micelles, solvent annealing causes only a few spherical micelles on SiO_x/Si to merge to form short cylindrical micelles, indicated by the coexistence of spherical (major) and cylindrical micelles (minor) on SiO_x/Si (Fig. 1h), but the short cylindrical micelles were immediately annihilated to form spherical micelles *via* fission upon further annealing (Fig. 1i and j). An abrupt disintegration of all spherical micelles to form a patchy layer is absent from SiO_x/Si during the entire solvent annealing when the substrate was completely covered with micelles. This behavior differs from the previous case of spherical micelles at a small coverage on SiO_x/Si, in which case solvent annealing led to dual layers. We explain the disparate structural evolution between the two cases of spherical micelles on SiO_x/Si as follows. As spun from a 0.5% solution, the substrate was fully covered with spherical micelles, so that no surface of the substrate was free from the spreading of micelles. At early stages of solvent annealing, in the presence of the attractive surface a-BCP chains from micelles adsorb at the substrate interface to form a wetting layer. During the formation of the wetting layer, if the micelles on top of the layer retained a critical size of aggregation, complete disintegration of micelles remained difficult and not practicable upon further solvent annealing. The micelles appear thus dispersed on a sea of a surface-induced ordered P(S-*b*-4VP) monolayer anchored on SiO_x/Si. Because fission dominated the growth of micellar species on SiO_x/Si with extended solvent annealing, spherical micelles spread over the entire free surface, as demonstrated in the AFM images (Fig. 1k and l). Spherical micelles with effective lateral ordering were obtained upon exposure of P(S-*b*-4VP) micelles to THF for 300 min.

Effects of end-grafting PS layers and size

As shown previously, the surface coverage plays an important role in the structural evolution of micelles on substrates particularly having interfacial interactions with the P4VP block. To shield from interfacial interactions between bare substrates and the P4VP block, we grafted bare silicon substrates with a layer of PS homopolymers. Here for surface grafting two PS homopolymers of disparate molar mass were used to explore the effect of various grafted PS lengths on the structural evolution of spherical micelles under solvent annealing. After end-grating PS (4 kg mol^{-1} or 19 kg mol^{-1}) onto SiO_x/Si, the effect of the surface coverage becomes trivial (comparing Fig. S3 in the ESI† and Fig. 2).

We performed also solvent annealing experiments on P(S-*b*-4VP) thin films that were prepared on spin-coating solutions of 0.5 mass% onto PS-grafted substrates. As shown in Fig. 2, before solvent annealing, all as-spun films again initially revealed the morphology of spherical micelles. Distinct morphological evolution was observed when initially disordered micelles on

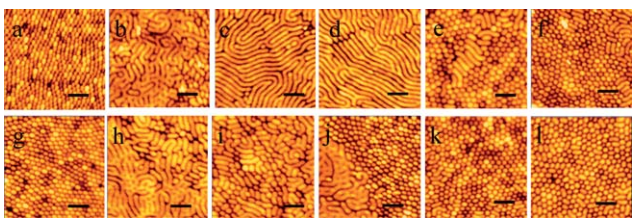

Fig. 2 AFM topographic images (1 μm × 1 μm) of P(S-*b*-4VP) thin films self-assembled on PS_{4k}–SiO_x/Si (a–f, top row) and PS_{19k}–SiO_x/Si (g–l, bottom row). Thin films were prepared on spin coating from a solution (0.5 mass%) in a toluene/THF solvent mixture. The topographic images were recorded (a and g) before and after P(S-*b*-4VP) films were subjected to solvent annealing for different periods: (b and h) 30, (c and i) 60, (d and j) 120, (e and k) 240, and (f and l) 300 min (scale bar: 200 nm).

This journal is © The Royal Society of Chemistry 2011

View Online

Published on 15 August 2011 on http://pubs.rsc.org | doi:10.1039/C1SM06082A
Downloaded by Synchrotron Radiation Library on 23 September 2011

PS_{4k}–SiO_x/Si and PS_{19k}–SiO_x/Si substrates were subjected to solvent annealing in THF. Short cylindrical micelles dominate the surface of PS-grafted substrates at an early stage of solvent annealing. After short-term annealing for ~30 min, short cylindrical micelles grew through merging of spherical micelles (Fig. 2b and h). After further exposure to THF vapors for 60 and 120 min, short cylindrical micelles on PS_{4k}–SiO_x/Si grew further into long cylinders *via* merging of short cylinders (Fig. 2c and d). Another growing trend of micelles on PS_{19k}–SiO_x/Si, showing the development of spherical micelles *via* fission of short cylindrical micelles at the intermediate stage, is, however, observable (Fig. 2i and j); long cylindrical micelles were not present on PS_{19k}–SiO_x/Si during solvent annealing. Spherical micelles eventually dominated the surface morphology on both grafted substrates instead (Fig. 2e, f and k, l).

To show quantitatively the temporal evolution of growth of micellar nanostructures during solvent annealing, we estimated fractions of cylindrical micelles per area of 2 μm × 2 μm. The reported cylindrical fractions represent an average over at least four measurements on separate 2 × 2 μm^2 areas for each sample. We considered only the quantitative analysis of the monolayer films as-spun from 0.5 mass% solutions because of their homogeneous surface coverage on substrates. Transitions from sphere to cylinder and from cylinder to sphere through fusion or fission are proposed through a detailed analysis of the fraction of cylindrical micelles per area using the Image J software, as quantitatively demonstrated in Fig. 3.

The upper curve (solid symbols) in Fig. 3 shows the fraction of cylindrical micelles as a function of time on PS_{4k}–SiO_x/Si; the lower group of curves (open symbols) shows the evolution on PS_{19k}–SiO_x/Si and SiO_x/Si. As shown in Fig. 3, at early stages of solvent annealing in THF, the growth curve of cylindrical micelles from the spherical micelles on PS_{4k}–SiO_x/Si through fusion is more rapid than on SiO_x/Si and PS_{19k}–SiO_x/Si. The surface coverage of the substrate with cylindrical micelles developed *via* fusion of spheres on PS_{4k}–SiO_x/Si is also greater.

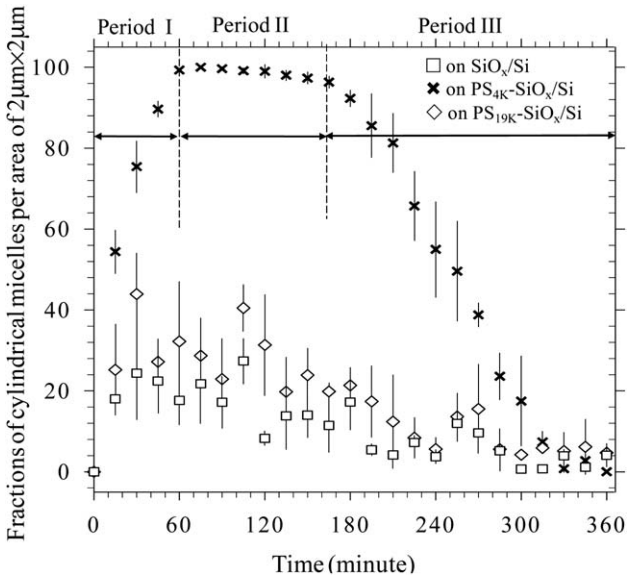

Fig. 3 Fractions of cylindrical micelles per area of 2 μm × 2 μm as a function of time for P(S-*b*-4VP) thin films on bare silicon substrates and substrates coated with end-grafting PS. The dotted lines are plotted to serve as a visual guide.

According to the morphological variation of P(S-*b*-4VP) micelles with the duration of solvent annealing in THF on PS_{4k}–SiO_x/Si, we identified three time periods (briefly denoted as periods I, II and III), in which inter-sphere fusion, inter-cylinder fusion or micellar fission dominates the micellar growth, respectively. Within period I (0–60 min), solvent annealing imparts the ability of P(S-*b*-4VP) spheres on PS_{4k}–SiO_x/Si to form short cylinders *via* inter-sphere fusion; both spheres and short nanocylinders thus coexist on top of PS_{4k}–SiO_x/Si. A complete transition to cylindrical micelles from spherical micelles on PS_{4k}–SiO_x/Si was obtained within 1 h. The fraction of cylindrical micelles on PS_{4k}–SiO_x/Si attained unity at 60 min. Subsequently the short cylinders fused with one another to grow long cylinders within period II, 60–150 min; the ordering of cylindrical micelles on PS_{4k}–SiO_x/Si became improved through inter-cylinder fusion. Cylindrical micelles remained stable, however, until the duration of solvent annealing reached 150 min, beyond which the cylindrical micelles became unstable and progressively transformed into spherical micelles though fission (period III). Within period III, the fission of micelles dominated over fusion. As a result, the fraction of spherical micelles increased with the duration of solvent annealing at the final stage. Upon further treatment the fraction of cylindrical micelles decreased exponentially until they vanished with solvent annealing for 300 min.

In contrast, throughout most solvent annealing in THF the fractions of cylindrical micelles developed though fusion on SiO_x/Si and PS_{19k}–SiO_x/Si was always less than those on PS_{4k}–SiO_x/Si. The growth curves of the cylindrical micelles on both SiO_x/Si and PS_{19k}–SiO_x/Si attained the maximum fraction at 30 min; at that point, cylindrical micelles were still present in minor amounts and spherical micelles were in major amounts. This result indicates that fission is dominant over fusion on SiO_x/Si and PS_{19k}–SiO_x/Si. As a result, the fraction of spherical micelles gradually increased with time after 30 min of solvent annealing. The entire surface covered with spherical micelles was eventually discerned because fission dominated in the growth of micellar species on SiO_x/Si and PS_{19k}–SiO_x/Si.

The morphologies of micelles depend strongly on the competition between fusion and fission. Experiments focused mainly on micellar evolution *via* fusion or fission of micelles in solution,[20,25,26] but there have been few investigations of the fusion or fission of micelles in thin films. We explain our observations on the basis of an improved understanding of the kinetic mechanism of the block copolymer self-assembly in solutions[25–28] as, to a certain degree, the micellar fusion or fission in thin films is conceptually analogous to that in solutions.[29,30] In the literature the length of PS corona chains and the incorporation of a precursor salt with the P4VP core block is reported to influence the rate of transitions between spherical and cylindrical micelles through fusion and fission.[23] In addition to these factors, here we find that both the length of the end-grafted layer and interfacial interactions are important factors in the transitions. The size effect of end-grafted PS is associated with various conformations of grafted polymers on a solid surface.[31] We observed surface morphologies by AFM. As shown in the AFM images of Fig. 4a and b, grafted PS_{4k} chains on SiO_x/Si reveal a featureless surface

View Online

Published on 15 August 2011 on http://pubs.rsc.org | doi:10.1039/C1SM06082A
Downloaded by Synchrotron Radiation Library on 23 September 2011

whereas grafted PS_{19k} chains display a rugged surface. This observation indicates that a smooth surface is attributed to a brush conformation whereas a rugged surface is associated with a mushroom conformation. In the dry state, these conformations may be possible. However, during the solvent annealing in THF vapor, both PS_{4k} and PS_{19k} grafted layers may have random-coiled structures if they are grafted with SiO_x/Si at a low density.[31] To acquire further insight into the conformations of grafted PS layers, we implemented characterizations with X-ray reflectivity. As shown in Fig. 4c and d, both the grafted PS layers clearly reveal a series of Kiessig fringes with one period. The wavelength of the fringes intrinsically depends on the thickness of grafted polymers on the solid surface. The curve-fitting result indicates that the grafted PS_{4k} layer has a thickness of 4 nm with a mean roughness of 0.33 nm; the grafted PS_{19k} layer has a thickness of 7.3 nm with a mean roughness of 0.56 nm. With this thickness information of the grafted layer, we calculate the grafted density using the equation[32]

$$\sigma = \rho d_0 N_A / M_n \quad (1)$$

in which d_0 represents the thickness of the grafted PS, the mass density of PS is denoted as ρ, and N_A represents the Avogadro constant and M_n is the number-averaged molar mass of PS. According to this estimation, the PS_{4k}-grafted layer was end-grafted at a density of 0.65 chains per nm^2 onto a solid surface, whereas the PS_{19k}-grafted layer had a density of 0.24 chains per nm^2. As the molar mass of short PS chains is less than M_e (the entanglement molar mass: 18.7 kg mol^{-1}),[33] an inter-chain entanglement is excluded. We speculate that, at such a grafted density of 0.65 chains per nm^2, the short grafted PS chains have the most probable conformations in a stretched state (as schematically illustrated in Fig. 4e), producing a smooth surface. Such a brush conformation of grafted chains prevents entanglement and interpenetration of PS chains between micelles and grafted brushes; no constraints on the fusion of micelles thus exist. For this reason the cylindrical micelles developed at a high rate of fusion on PS_{4k}–SiO_x/Si.

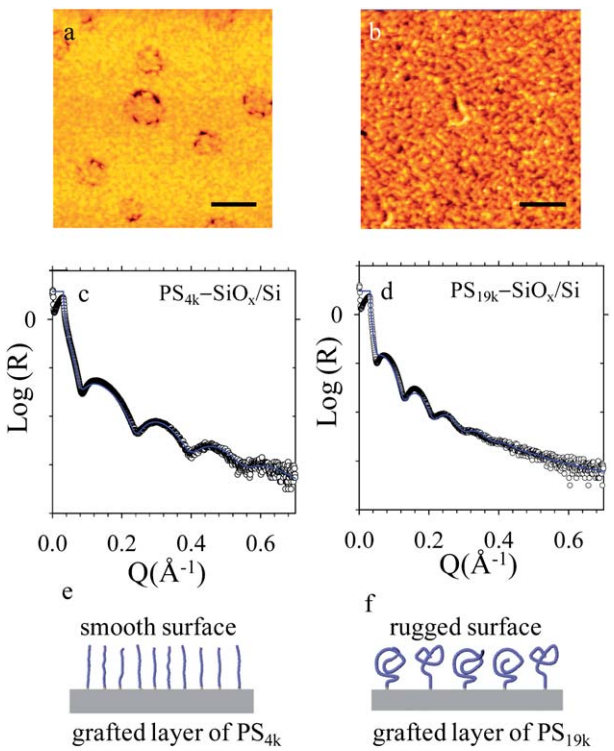

Fig. 4 (a and b) AFM topographic images (1 μm × 1 μm) and (c and d) X-ray reflectivity profiles of grafted PS_{4k} and PS_{19k} layers on a substrate. Symbols represent experimental data and lines represent their fitted curves. (e and f) Schematic illustrations of the surface contour of the grafted layer of PS_{4k} and PS_{19k}.

Because of a small grafted density and long chains with molar mass greater than M_e, the grafted PS_{19k} layer is expected to be more likely in a mushroom-like conformation (as schematically illustrated in Fig. 4f) rather than in a brush-like conformation. The mushroom-like conformation of long grafted chains thus produced the rugged surface evident in the AFM image. The micelle fusion has been shown to depend on the probability of collisions.[27,28] In solvent-annealed thin films, the solvent vapors impart the ability of motion for micelles to collide to fuse during solvent annealing. The degree of mobility of micelles determines the rate at which they move to contact and collide with their neighbors. On top of a grafted layer of PS_{19k} chains in the mushroom-like conformation, the rugged surface increases the energy barrier for motion of micelles to approach neighbors.[34,35] The slow dynamics for polymers in contact with substrates at rugged surfaces might account for the retarded rate of fusion of micelles. The reason is that close micelle–micelle contacts to fuse together through migration of micelles are more difficult on a grafted layer of PS_{19k} with a rugged surface than on a smooth layer of dense PS_{4k} brushes.

The effective volume fraction of the PS block increases with the duration of solvent annealing due to continuous swelling of the PS block by THF. The more the solvent selectively swells one block, the more asymmetric the volume fraction of the P(S-*b*-4VP) a-BCP becomes. The time scale for forming spherical micelles from fission of cylindrical micelles is much smaller on PS_{19k}–SiO_x/Si than on PS_{4k}–SiO_x/Si because the fusion of micelles on PS_{19k}–SiO_x/Si is retarded. As a result, forming spherical micelles is more favored than forming cylindrical micelles in P(S-*b*-4VP) thin films on PS_{19k}–SiO_x/Si.

We proceed to interpret why spherical micelles always dominate over cylindrical micelles on SiO_x/Si for thin films of approximately monolayer thickness during the entire solvent annealing. For as-spun spherical micelles on SiO_x/Si, the attractive surface causes adsorption of some P(S-*b*-4VP) chains from micelles to the substrate surface, forming a wetting layer at the interface during solvent annealing. As THF is an effective solvent for PS but a poor solvent for P4VP, unfavorable P4VP–solvent interactions also drive the adsorption of a layer of P(S-*b*-4VP) chains with SiO_x/Si. A similar adsorption of BCP micelles at interfaces in the presence of the solvent was experimentally observed in other BCP systems.[36] For the wetting layer of P(S-*b*-4VP) chains, the P4VP block bound to the surface is denoted as the anchor block whereas the swollen PS block stretching away from the surface acts as a tail. Although an unfavorable contact of the P4VP block with THF drives shrinkage of the P4VP anchoring chain, the size of the P4VP anchoring block is larger than that of the hydrophilic head for hydroxyl-terminated polystyrene homopolymers. The wetting layer of P(S-*b*-4VP)

 This journal is © The Royal Society of Chemistry 2011

View Online

Published on 15 August 2011 on http://pubs.rsc.org | doi:10.1039/C1SM06082A
Downloaded by Synchrotron Radiation Library on 23 September 2011

chains is expected to anchor on SiO_x/Si at a low density, increasing free space for occupation by the P4VP core chains of the wetting layer so that PS chains might have a mushroom-like conformation rather than a brush-like conformation. Fig. S2f (ESI†) reveals that the anchoring P(S-*b*-4VP) layer (*ca.* 4 nm) is thinner than the grafted layer of PS_{19k}, even though the symmetric P(S-*b*-4VP) has nearly twice the molar mass of PS_{19k}. This result indicates that the anchoring density of P(S-*b*-4VP) chains adsorbed at SiO_x/Si is much less than the grafting density of long PS chains covalently bonded with SiO_x/Si.

At such a small anchoring density, it is highly possible that interpenetration and entanglement exist between a-BCP chains within micelles and a-BCP chains within the underlying layer adsorbed at the substrate interface. If the top monolayer of micelles is interpenetrated and entangled with the anchoring layer underneath, they act as tethered micelles; their motion thus becomes constrained by the underlying layer. In this case, the constrained motion of tethered micelles significantly retards micellar merger. To identify whether interpenetration and entanglement exist for micelles on bare substrates during solvent annealing, we conducted a simple experiment of lifting off to remove micelles through sonication (40 min) of the film-covered substrates in toluene or THF after films were subjected to protracted annealing under solvent vapors. If micelles are tethered on SiO_x/Si by interpenetration and entanglement, removing of a-BCP micelles from bare substrates by lifting off might be difficult to achieve within tens of minutes. For comparison, the lifting-off experiment was imposed also on homogeneous films that uniformly covered PS-grafted substrates. The AFM topographic image of Fig. 5a reveals a dumbbell-like morphology, indicative of deformed micelles of P(S-*b*-4VP). This result indicates that sonication in toluene for 40 min to remove micelles from bare substrates is not achievable. The difficulty of lifting off a-BCP micelles on SiO_x/Si implies the existence of interpenetration and entanglement of the anchoring layer onto micelles. The micelles are hence in sticky contact with the anchoring layer. In contrast, after the same lifting off, no micelle stays on top of a dense layer of PS_{4k} brushes, evident from a featureless surface, as shown in Fig. 5b. This result indicates that the dense layer of PS_{4k} prevents penetration of P(S-*b*-4VP) chains within micelles. No interpenetration and entanglement of the polymer brush into the a-BCP micelles thus occurred in the case of micelles on PS_{4k}–SiO_x/Si. In comparison, still few micelles remain on top of PS_{19k}–SiO_x/Si (Fig. 5c). The degree of penetration and entanglement clearly depends on the anchor or graft density: the smaller is this density, the greater is the degree of interpenetration and entanglement.

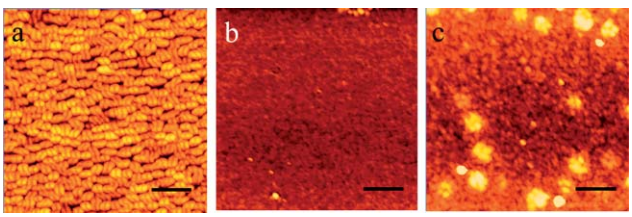

Fig. 5 AFM topographic images (1 μm × 1 μm) for surface morphologies of (a) SiO_x/Si, (b) PS_{4k}–SiO_x/Si and (c) PS_{19k}–SiO_x/Si after thin films were annealed in THF for at least 10 h and then subjected to sonication in toluene for 40 min.

This explanation accounts also for the fact that the retardation of micellar fusion is more evident on SiO_x/Si.

Nanopores and nanogrooves developed with solvent annealing in THF combined with surface construction in ethanol

Fig. 6a and b show the 45°-tilted FESEM images for the cross-sectional morphology of surface-reconstructed P(S-*b*-4VP) films on SiO_x/Si and PS_{4k}–SiO_x/Si, respectively. Before the FESEM characterizations, surface-constructed films on SiO_x/Si and PS_{4k}–SiO_x/Si were prepared on solvent annealing in THF for 120 min followed by immersion in ethanol (effective solvent for the P4VP block) for 20 min. Treating monolayered P(S-*b*-4VP) films by immersion in ethanol led to confined swelling-induced pore generation, consequently yielding opened micelles.[37–39] The preceding AFM images reveal that, with solvent annealing in THF for 120 min, long cylindrical micelles predominantly cover the surface of PS_{4k}–SiO_x/Si whereas spherical micelles predominate on top of SiO_x/Si. The FESEM images show that the film on SiO_x/Si reveals hexagonally arranged nanoporous arrays whereas the film on PS_{4k}–SiO_x/Si reveals corrugated nanogrooves. The presence of holes and corrugated grooves upon immersion in ethanol is due to selective migration of the P4VP block onto the free surface of the film.[3,16,37–39] The nanopores and corrugated nanogrooves thus have a depth that is nearly comparable with the film thickness. On examination of the strip-like nanostructures for the P(S-*b*-4VP) film on PS_{4k}–SiO_x/Si, we observed the presence of hemispherical caps at ends of the strips. This observation indicates that the stripe-like nanogrooves shown in the cross-sectional FESEM image of the P(S-*b*-4VP) on PS_{4k}–SiO_x/Si resulted from the surface-reconstruction of parallel-oriented nanocylinders rather than from vertical nanolamellae.

As shown in Fig. 6c and d, the corresponding 2D GISAXS pattern for P(S-*b*-4VP) on SiO_x/Si reveals sharp diffraction-

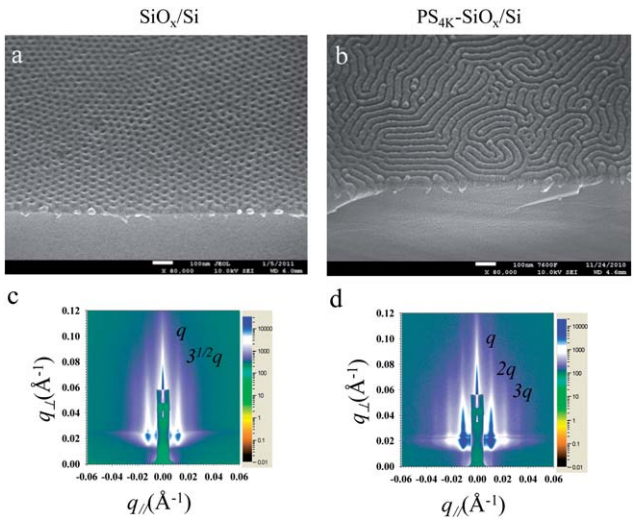

Fig. 6 45°-Tilted FESEM images of a P(S-*b*-4VP) thin film on (a) SiO_x/Si (left image) and (b) PS_{4k}–SiO_x/Si (right image). Both samples were solvent-annealed in THF for 120 min and then immersed in ethanol for 20 min to enhance the topographic contrast through surface reorganization before FESEM characterizations. The corresponding GISAXS patterns of P(S-*b*-4VP) thin films on SiO_x/Si (c) and PS_{4k}–SiO_x/Si (d).

View Online

truncated rods located at $q_{\|}$ ratios $1 : 3^{1/2}$ with respect to the position ($q_{\|} = 0.0138$ Å^{-1}) of the principal rod whereas these features with $q_{\|}$ ratios $1 : 4^{1/2} : 9^{1/2}$ are clearly discerned for P(S-*b*-4VP) on PS_{4k}–SiO_x/Si. A comparison between the two GISAXS patterns indicates that the rod at $q_{\|} = 0.0239$ Å^{-1} that corresponds to the $q_{\|}$ ratio $3^{1/2}$ with respect to the position of the principal Bragg rod is absent for P(S-*b*-4VP) on PS_{4k}–SiO_x/Si. This $3^{1/2}$ rod typically associated with diffraction of the {11} plane is observable only for ordered structures with a hexagonal packing.[40] The forbidden diffraction might, however, be due to the fact that a single monograin of nanopores revealed the angular dependence of reflections on rotating a sample with respect to the incident direction of X-rays.[40] As the FESEM image of P(S-*b*-4VP) nanodomains on SiO_x/Si reveals hexagonal arrays with in-plane polygrains, we exclude the existence of a single monograin in the case of P(S-*b*-4VP) on SiO_x/Si. Thus, the absence of the $3^{1/2}$ peak is taken to indicate that parallel P4VP nanocylinders on PS_{4k}–SiO_x/Si lack hexagonal order within the PS matrix.[41] The GISAXS result demonstrates that, upon solvent annealing in THF combined with immersion in ethanol, P(S-*b*-4VP) nanodomains on SiO_x/Si exist as nanopores in a hexagonal array within a PS matrix whereas they exist as nanogrooves with respect to the surface of PS_{4k}–SiO_x/Si.

Hierarchical self-assembly of micelles on a micro-patterned substrate

These experimental results indicate that the kinetics of micellar transitions *via* fusion or fission are influenced by the grafted layer on a solid surface. To achieve a hierarchical assembly of micellar nanostructures, we applied chemical patterning.[42,43] Fig. 7A shows the scheme for the fabrication of chemically patterned substrates utilizing UV light and ozone for selective etching of the grafted layer of PS_{4k}, in which a TEM copper grid served as an etching mask. In unetched areas, the PS_{4k} chains remained end-grafting with SiO_x/Si whereas, in etched areas, the grafted PS chains without protection from the TEM grid were selectively degraded with UV light and ozone. By selective removal of the grafted PS, the areas that were exposed to UV light and ozone have a hydrophilic surface. Next, we spin-coated spherical micelles on the chemically patterned substrate, and implemented solvent annealing in THF for 90 min. To induce dimple-like nanopores and stripe-like nanogrooves *via* surface reconstruction from spherical and cylindrical micelles, the solvent-annealed film was immersed in ethanol for 20 min before FESEM characterizations. Fig. 7B shows the development of a globally ordered P(S-*b*-4VP) copolymer with a hierarchical assembly, which replicates the pattern of a TEM copper grid. The presence of the micro-pattern on the P(S-*b*-4VP) thin film is attributed to the morphological contrast from the coexistence of nanopores and nanogrooves. Fig. 7C shows that unetched regions under the shadow of the TEM grid display stripe-like nanogrooves, indicative of the rapid development of parallel cylindrical nanodomains through fusion on top of a grafted layer of PS_{4k} brushes. In contrast, Fig. 7D shows that the discrete squared regions from selective removal of the underlying PS layer display dimple-like nanopores at the same duration of solvent annealing. The FESEM image of Fig. 7E shows the coexistence of dimple-like nanopores and stripe-like nanogrooves at the boundary between

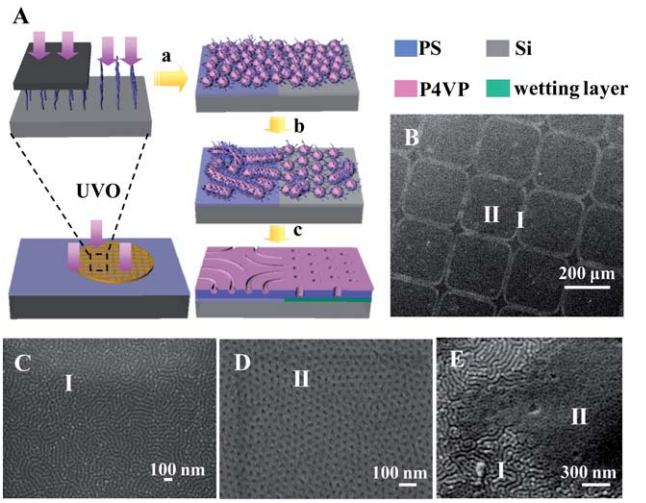

Fig. 7 (A) Schematic illustration of a hierarchically self-assembled thin film on a chemically micro-patterned substrate. The chemical micropatterning of a PS_{4k}-grafted substrate was fabricated through selective etching of the grafted PS layer by UV light and ozone. Both dimple-like nanopores and stripe-like nanogrooves coexist within the same monolayer for sample treatments in a sequence: (a) deposition of spherical micelles, (b) solvent annealing in THF, and (c) surface reconstruction with immersion in ethanol. (B) Slightly and (C–E) highly magnified FESEM images of a monolayered micelle block-copolymer film self-assembled on a chemically patterned PS layer. Region I was protected against UV/ozone etching with the Cu TEM grid, whereas region II was etched. The FESEM image of the former region reveals stripe-like nanogrooves (C), whereas the FESEM image of the latter region reveals nanopores packed in a hexagonal lattice (D). (E) Both dimple-like nanopores and stripe-like nanogrooves coexist.

etched and unetched regions. This result indicates that, upon combining the chemical micropatterning of the grafted PS layer with UV light and ozone etching, we prepared P(S-*b*-4VP) films that have nanopores and nanogrooves coexisting with a micrometer-scale order within the same monolayer.

Conclusions

Grafting a layer of short PS chains on top of Si substrates to shield effectively interfacial interactions between the P4VP block and the attractive surface of bare Si substrates significantly facilitates the extent and rate of micellar fusion. At the early and intermediate stages of solvent annealing, cylindrical micelles are dominant over spherical micelles on a dense layer of short brushes. On substrates having an attractive surface or a grafted layer of long PS chains, upon solvent annealing, the major domain within thin monolayered films is still spherical micelles because of the retardation of micellar fusion according to which spherical micelles merge to form cylindrical micelles. We ascribe the retardation of micellar fusion to the presence of entanglement and interpenetration of micelles with the underlying chains in a mushroom-like conformation. The spherical micelles became the only discernible species when monolayered films were exposed to THF for durations longer than 300 min regardless of the bare or grafted substrates, which indicates that at the final stage the spherical micelles are favored due to the dominance of micellar fission.

Published on 15 August 2011 on http://pubs.rsc.org | doi:10.1039/C1SM06082A
Downloaded by Synchrotron Radiation Library on 23 September 2011

This journal is © The Royal Society of Chemistry 2011

View Online

We demonstrated also a kinetic method to develop the hierarchical self-assembly of block copolymer micelles. The hierarchical assembly was achieved upon control of the fusion and fission of micelles on a chemically patterned substrate that was fabricated on selective removal of PS brushes on exposure to ultraviolet light and ozone. The main advantage of kinetically controlled hierarchical ordering of micelles by means of chemical patterning upon solvent annealing is to offer an ability to achieve the coexistence of opened spherical and cylindrical micelles within the same layer of films. Since the hierarchical self-assembly of P(S-*b*-4VP) micelles was kinetically achieved on simply controlling the duration of annealing under solvent vapor, the hierarchical ordering upon solvent annealing micelles on a chemically patterned substrate was thus achieved within a brief period.

Acknowledgements

National Science Council provided support (NSC-99-2221-E-008-009 and NSC-98-2120-M-008-004). The authors are grateful to Prof. Bao-Tsan Ko of Chung Yuan Christian University, who kindly supplied the PS19k-OH. We thank Dr U-Ser Jeng, Dr Chiu-Hun Su and Dr Chun-Jen Su for their assistance in the GISAXS experiments at beamline BL23A at the NSRRC, and Mr Er-Chiang Chen for the assistance in measuring X-ray reflectivity at National Chung-Hsing University. Y.S.S. also thanks Ms S.-C. Chi of the Regional Instrument Center at NTU for her assistance in the FESEM experiments.

References

1 Y. Qiao, D. Wang and J. M. Buriak, *Nano Lett.*, 2007, **7**, 464.
2 S. Park, J.-Y. Wang, B. Kim and T. P. Russell, *Nano Lett.*, 2008, **8**, 1667.
3 S. Park, B. Kim, J.-Y. Wang and T. P. Russell, *Adv. Mater.*, 2008, **20**, 681.
4 M. Aizawa and J. M. Buriak, *J. Am. Chem. Soc.*, 2005, **127**, 8932.
5 M. Aizawa and J. M. Buriak, *Chem. Mater.*, 2007, **19**, 5090.
6 Y. Kim, H. Han, Y. Kim, W. Lee, M. Alexe, S. Baik and J. K. Kim, *Nano Lett.*, 2010, **10**, 2141.
7 S.-H. Yun, S. I. Yoo, J. C. Jung, W.-C. Zin and B.-H. Sohn, *Chem. Mater.*, 2006, **18**, 5646.
8 H.-G. Boyen, G. Kästle, K. Zürn, T. Herzog, F. Weigl, P. Ziemann, O. Mayer, C. Jerome, M. Möller, J. P. Spatz, M. G. Garnier and P. Oelhafen, *Adv. Funct. Mater.*, 2003, **13**, 359.
9 J. P. Spatz, V. Z.-H. Chan, S. Möβmer, F. M. Kamm, A. Plettl, P. Ziemann and M. Möller, *Adv. Mater.*, 2002, **14**, 1827.
10 T. Lohmueller, E. Bock and J. P. Spatz, *Adv. Mater.*, 2008, **20**, 2297.
11 J. Chai and J. M. Buriak, *ACS Nano*, 2008, **2**, 489.
12 K.-V. Peonemann, V. Abetz and P. F. W. Simon, *Nat. Mater.*, 2007, **6**, 992.
13 S. Förster and M. Antonietti, *Adv. Mater.*, 1998, **10**, 195.
14 S. Förster and T. Plantenberg, *Angew. Chem., Int. Ed.*, 2002, **41**, 688.
15 S. P. Numes, R. Sougrat, B. Hooghan, D. H. Anjum, A. R. Behzad, L. Zhao, N. Pradeep, I. Pinnau, U. Vainio and K.-V. Peinemann, *Macromolecules*, 2010, **43**, 8079.
16 S. Park, B. Kim, J. Xu, T. Hofmann, B. M. Ocko and T. P. Russell, *Macromolecules*, 2009, **42**, 1278.
17 S. Park, J.-Y. Wang, B. Kim, W. Chen and T. P. Russell, *Macromolecules*, 2007, **40**, 9059.
18 S. Park, J.-Y. Wang, B. Kim, J. Xu and T. P. Russell, *ACS Nano*, 2008, **2**, 766.
19 S. Park, B. Kim, O. Yavuzcetin, M. T. Tuominen and T. P. Russell, *ACS Nano*, 2008, **2**, 1363.
20 G. Riess, *Prog. Polym. Sci.*, 2003, **28**, 1107.
21 B. Nandan, E. B. Gowd, N. C. Bigall, A. Eychmüller, P. Formanek, P. Simon and M. Stamm, *Adv. Funct. Mater.*, 2009, **19**, 2805.
22 E. B. Gowd, B. Nandan, M. K. Vyas, N. C. Bigall, A. Eychmüller, H. Schlörb and M. Stamm, *Nanotechnology*, 2009, **20**, 415302.
23 T. H. Kim, J. Huh, J. Huang, H.-C. Kim, S. H. Kim, B.-H. Sohn and C. Park, *Macromolecules*, 2009, **42**, 6688.
24 U. S. Jeng, C. H. Su, C. J. Su, K. F. Liao, W. T. Chuang, Y. H. Lai, J. W. Chang, Y. J. Chen, Y. S. Huang, M. T. Lee, K. L. Yu, J. M. Lin, D. G. Liu, C. F. Chang, C. Y. Liu, C. H. Chang and K. S. Liang, *J. Appl. Crystallogr.*, 2010, **43**, 110.
25 R. C. Hayward and D. J. Pochan, *Macromolecules*, 2010, **43**, 3577.
26 A. G. Denlova, E. Mendes and M.-O. Coppens, *Soft Matter*, 2010, **6**, 2351.
27 F. J. Esselink, E. E. Dormidontova and G. Hadziioannou, *Macromolecules*, 1998, **31**, 4873.
28 F. J. Esselink, E. E. Dormidontova and G. Hadziioannou, *Macromolecules*, 1998, **31**, 2925.
29 M. Munch and A. P. Gast, *Macromolecules*, 1998, **21**, 1360.
30 M. Munch and A. P. Gast, *Macromolecules*, 1998, **21**, 1366.
31 B. Zhao and W. J. Brittain, *Prog. Polym. Sci.*, 2000, **25**, 677.
32 X. Zhang, F. K. Lee and O. K. C. Tsui, *Macromolecules*, 2008, **41**, 8148.
33 J. E. Mark, *Physical Properties of Polymers Handbook*, American Institute of Physics, New York, USA, 1996.
34 S. Santer, A. Kopyshev, J. Donges, H.-K. Yang and J. Rühe, *Adv. Mater.*, 2006, **18**, 2359.
35 G. D. Smith, D. Bedrov and O. Borodin, *Phys. Rev. Lett.*, 2003, **90**, 226103.
36 M. Munch and A. P. Gast, *Macromolecules*, 1990, **23**, 2313.
37 Y. Wang and F. Li, *Adv. Mater.*, 2011, **23**, 2134.
38 B. H. Sohn, S. I. Yoo, B. W. Seo, S. H. Yun and S. M. Park, *J. Am. Chem. Soc.*, 2001, **123**, 12734.
39 Z. Chen, C. He, F. Li, L. Tong, X. Liao and Y. Wang, *Langmuir*, 2010, **26**, 8869.
40 S. Park, D. H. Lee, J. Xu, B. Kim, S. W. Hong, U. Jeong, T. Xu and T. P. Russell, *Science*, 2009, **323**, 1030.
41 Y.-S. Sun, S.-W. Chien and J.-Y. Liou, *Macromolecules*, 2010, **43**, 7250.
42 S.-J. Jeong, G. Xia, B. H. Kim, D. O. Shin, S.-H. Kwon, S.-W. Kang and S. O. Kim, *Adv. Mater.*, 2008, **20**, 1898.
43 B. H. Kim, J. Y. Kim, S.-J. Jeong, J. O. Hwang, D. H. Lee, D. O. Shin, S.-Y. Choi and S. O. Kim, *ACS Nano*, 2010, **4**, 5464.

Published on 15 August 2011 on http://pubs.rsc.org | doi:10.1039/C1SM06082A
Downloaded by Synchrotron Radiation Library on 23 September 2011